Optics Letters

Vortex degeneracy lifting and Aharonov–Bohm-like interference in deformed photonic graphene

Peng Zhang,[1,2] Daniel Gallardo,[1] Sheng Liu,[1,3] Yuanmei Gao,[1,4] Tongcang Li,[2] Yuan Wang,[2] Zhigang Chen,[1,5,7] and Xiang Zhang[2,6,8]

[1]Department of Physics and Astronomy, San Francisco State University, San Francisco, California 94132, USA
[2]National Science Foundation Nanoscale Science and Engineering Center, University of California, 3112 Etcheverry Hall, Berkeley, California 94720, USA
[3]The MOE Key Laboratory of Space Applied Physics and Chemistry and School of Science, Northwestern Polytech. University, Xi'an 710072, China
[4]College of Physics and Electronics, Shandong Normal University, Jinan 250014, China
[5]The MOE Key Laboratory of Weak-Light Nonlinear Photonics and School of Physics, Nankai University, Tianjin 300457, China
[6]Materials Sciences Division, Lawrence Berkeley National Laboratory, 1 Cyclotron Road, Berkeley, California 94720, USA
[7]e-mail: zhigang@sfsu.edu
[8]e-mail: xiang@berkeley.edu

Received 3 November 2016; revised 6 January 2017; accepted 7 January 2017; posted 12 January 2017 (Doc. ID 279691); published 20 February 2017

Photonic graphene, a honeycomb lattice of evanescently coupled waveguides, has provided a superior platform for investigating a host of fundamental phenomena such as unconventional edge states, synthetic magnetic fields, photonic Landau levels, Floquet topological insulators, and pseudospin effects. Here, we demonstrate both experimentally and numerically, topological vortex degeneracy lifting and Aharonov–Bohm-like interference from local deformation in a photonic honeycomb lattice. When a single valley is excited, lattice deformation leads to the generation of a vortex pair due to the lifting of degeneracy associated with pseudospin states. In the case of double-valley excitation, we observe the Aharonov–Bohm-like interference merely due to the deformation of the graphene lattice, which gives rise to an artificial gauge field. Our results may provide insight into the understanding of similar phenomena in other graphene-like materials and structures.
© 2017 Optical Society of America

OCIS codes: (160.5293) Photonic bandgap materials; (130.2790) Guided waves; (080.4865) Optical vortices.

https://doi.org/10.1364/OL.42.000915

Since graphite monolayers were first isolated in a controlled way, graphene has attracted an ever increasing interest due to its striking electronic, structural, and mechanical properties as an extraordinary two-dimensional material, as well as the many intriguing fundamental phenomena mediated by its unique bandgap structure, including the anomalous quantum Hall effect, Klein tunneling, and the absence of back scattering [1–3]. Indeed, much of the underlying physics arises from the special symmetry and linear band dispersion of the graphene honeycomb lattices (HCLs), which has drawn interest in exploring artificial HCLs as a platform to mimic the transport dynamics of massless Dirac fermions in natural carbon-based graphene. Such "artificial graphene" [4] has been proposed and demonstrated in a number of settings, including photonic lattices [5,6]. The motivation for studying this artificial graphene is that they can be easily accessed, even in regimes where it is difficult or impossible for natural graphene. It has been demonstrated that graphene-like optical lattices loaded with ultracold atoms could be employed for measuring geometric phases with high momentum resolution, enabling full characterization of Bloch band topology [7,8].

One of the intriguing phenomena that has also attracted interdisciplinary interest is "strain engineering" and associated effects arising from synthetic magnetic fields (gauge fields). It was theoretically proposed that strain can be used to engineer graphene electronic states by inducing a synthetic field, leading to a pseudo-magnetic quantum Hall effect [9]. Such strain-induced pseudo–magnetic fields, greater than 300 T, were successfully demonstrated in graphene nanobubbles, exhibiting the expected scaling behavior for Landau levels in graphene [10]. It has also been suggested that even in the limit of a weak gauge field, non-trivial fundamental effects, such as the Aharonov–Bohm (AB) interferences from local deformations in graphene, can be realized [11]. Meanwhile, artificial gauge fields have been the subject of intensive research in ultracold atoms [12–14] and in photonics [15–18].

Photonic graphene [5], a honeycomb array of evanescently coupled waveguides, has proven to be particularly useful for investigating graphene physics in various optical settings

[19–27]. The photonic analogy of graphene arises not only due to the HCL structure, but also the similarity between the paraxial equation describing light propagation in HCLs and the Schrödinger equation for electrons in graphene. The HCLs can be conveniently established in optical materials, either by nonlinear optical induction or by the femtosecond laser writing [23], in which the Bloch modes with a desired momentum can be selectively excited, and the wavefunction including the phase can be directly measured. This has led to the direct observation of a host of interesting phenomena in photonic graphene, including unconventional edge states, strain-induced pseudomagnatic fields and photonic Landau levels, photonic Floquet topological insulators, and pseudospin-mediated vortices generation [23–27]. Inspired by the theoretical prediction [11] that the AB interference [28] can occur from local deformations in real carbon-based graphene and the experimental demonstration of pseudomagnetic effect in a strained artificial photonic graphene [25], one may wonder if the AB interference can be observed in photonic graphene by applying deformation to the optically induced HCLs.

In this Letter, we demonstrate deformation-induced vortex degeneracy lifting and Aharonov–Bohm-like interference in an optically induced photonic honeycomb lattice. Specifically, by using a simple yet effective method, we can generate photonic graphene lattices with desired local index deformation. By sending a probe beam with its momentum matched onto one of the K valleys, both sublattices are equally excited so no topological vortex is created due to the degeneracy of pseudospin states. However, by adding a deforming beam to induce index deformation in the HCLs, a pair of vortices is observed in the probe beam due to the degeneracy lifting of vortices. Moreover, by sending two probe beams to excite two equivalent K valleys, we observe a phase shift in the vortex interferogram from the Bragg-reflected component before and after introducing deformation, analogous to the predicted AB interference from deformation in graphene.

Our experimental setup used for optical induction and deformation of photonic graphene is illustrated in Fig. 1. A two-dimensional HCL is induced in a biased photorefractive crystal (SBN:60) by sending an ordinarily polarized diffused laser beam (488 nm) through an amplitude mask, as used in our earlier work [27,29]. After imaging the mask onto the input facet of the crystal, a HCL pattern is created and sent through the crystal. By employing a proper spatial bandpass filter at the Fourier plane of the mask, the Talbot self-imaging effect can be totally eliminated, so that the partially coherent HCL pattern remains invariant during the propagation throughout the crystal (blue path). With a proper electric bias field, this intensity pattern induces quasi-periodic index changes in the otherwise uniform crystal, forming a honeycomb waveguide array or index lattice. To introduce deformations in the lattice structure, a relatively broad Gaussian beam (also ordinarily polarized) is sent through another rotating diffuser, propagating collinearly with the lattice beam (green path). This Gaussian beam could also be focused to detect the Brillouin zone (BZ) spectrum [30]. In addition, an extraordinarily polarized Gaussian beam (or a pair of Gaussian beams selected from a three-beam interference pattern) is used as a probe, which is momentum matched to the targeted valleys of the graphene lattice (red path). The near-field and far-field patterns of the lattice-inducing and probe beams are monitored with imaging lenses and a CCD camera.

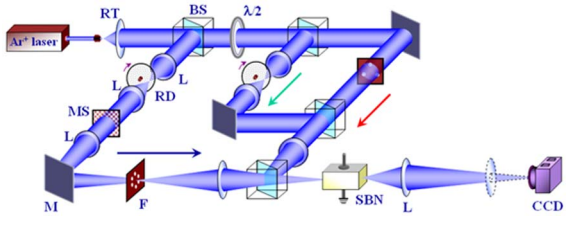

Fig. 1. Schematic of the experimental setup for generation and probing of a photonic HCL with local deformation. RT, reversed telescope; RD, rotating diffuser; BS, beam splitter; L, lens; MS, amplitude mask; M, mirror; F, spatial bandwidth filter; SBN, strontium barium niobate. The blue path is for optically inducing a uniform honeycomb photonic lattice; the green path is for introducing local deformation in the lattice; the red path is for probing the lattice with a single (or double) beam momentum matched to a single (double) valley.

Typical numerical and experimental results of the photonic graphene lattice, its BZ spectrum, as well as a Gaussian-beam induced nonuniform deformation, are presented in Fig. 2. By fine-tuning the weak nonlinearity experienced by the ordinarily polarized lattice-inducing beam (as controlled by the beam intensity, coherence, as well as the bias field), a HCL of index modulation is established [Figs. 2(a) and 2(e)]. The BZ spectrum measured with a partially incoherent probe beam [Fig. 2(f)] matches perfectly with that obtained from a numerical calculation [Fig. 2(b)], where K marks one of the six Dirac points, as shown in Fig. 2(g) [see also Fig. 2(c) for the band diagram centered on the K valley]. In the right two panels [Figs. 2(d) and 2(h)], a broad Gaussian beam (see the inserts) is added to the lattice induction, which results in a local deformations in the otherwise uniform photonic graphene, as theoretically proposed for deforming a sheet of graphene to demonstrate the AB interference [11]. Since the lattice beam is nondiffracting and the Gaussian beam is loosely focused, the deformed graphene lattice remains invariant along the 10 mm long crystal.

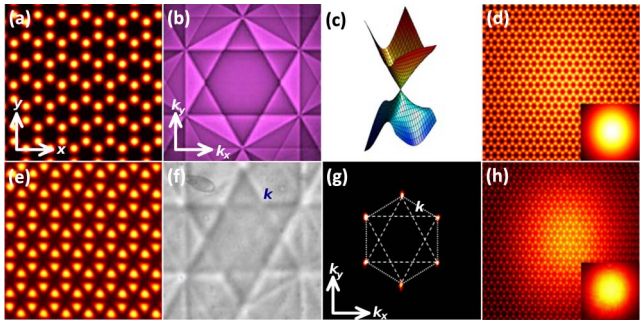

Fig. 2. Optically induced uniform (left column) and deformed (right column) photonic HCL. (a)–(d) Numerical simulation results of the lattice structure, Brillouin zone spectrum, band structure near the Dirac point, and the deformed lattice (the deforming beam at input is shown in the inset). The corresponding experimental results of (a), (b), and (d) are presented in (e), (f), and (h), where the measured BZ spectrum agrees well with the calculated spectrum. (g) Schematic of the first BZ of the induced lattice, with six bright spots representing measured spectrum of the lattice. To selectively excite a one-set valley point with an identical "spin" property, the input beam is momentum matched to the corresponding K points in the BZ of the lattice.

We first look into the case of single-beam excitation of a single valley in a uniform graphene lattice, as shown in Fig. 3. To selectively excite a valley, the spectrum of the input probe beam is set to overlap with the corresponding K point in the BZ of the lattice. As shown in Figs. 3(a) and 3(e), when a single valley (marked as K) is initially excited, two new spectral components are generated at the other two K valleys due to Bragg reflection. [Note that Figs. 3(a) and 3(e) are the output spectra of the probe beam, while at the input only a single valley is initially excited.] Taking one of the Bragg-reflected components and performing an inverse Fourier transform to the real space, we could not identify any topological charge in the interferograms [Figs. 3(c) and 3(g)]. The phase diagram from numerical simulation shows no net vorticity [Fig. 3(d)], and the interference from two Bragg-reflected components measured from the experiment also shows no phase singularity [Fig. 3(h)]. This is not surprising from the viewpoint of pseudospin states [27,31,32]: different pseudospin states can be excited, depending on the initial position of the probe beam relative to the HCL. If the probe beam only selectively excites either sublattice A or sublattice B, a pseudospin state is revealed corresponding to a topological charge generation. In contrast, if the probe beam excites both sublattices simultaneously, opposite pseudospin states are equally excited which leads to no net vorticity. The results in Fig. 3 correspond to this latter case: a single Gaussian beam excites both sublattices equally, which does not result in any net vorticity due to lattice pseudospin; thus, no fringe bifurcation in the interferogram is observed. Note that the apparent difference between the output patterns from the numerical simulation [Fig. 3(b)] and the experiment [Fig. 3(f)] is mainly due to the deviation of experimental conditions from those used in simulations.

In contrast, in a nonuniformly deformed HCL lattice (strained photonic graphene), the same single-beam excitation leads to dramatically different behavior. For direct comparison, the corresponding results are shown in Fig. 4, with all experimental conditions the same as in Fig. 3, except for adding the deforming beam. In this case, one can clearly see the generation of a pair of vortices with opposite vorticity, indicating that the vortex (pseudospin) degeneracy is lifted due to lattice deformation. Intuitively, one might understand this from the deformation-induced gauge field in graphene [33]. The gauge field due to lattice deformation induces a small energy gap near the Dirac points, so the two opposite pseudospin states associated with the two sublattices are separated, leading to the lifting of the pseudospin-mediated vortex degeneracy. The underlying mechanism certainly merits further theoretical investigation.

To demonstrate the Aharonov–Bohm interference in deformed photonic graphene, we create an interference scheme so that two light waves are incoming from a geometrically identical path [11,28]. Since our probe beam comes from the amplitude mask (with three holes) which could generate one set of the triangular lattices corresponding to the graphene lattice (see Fig. 1), we can simply use only two beams, momentum matched to two K valleys. Then these two beams will pass through the lattice structure and be Bragg reflected at the third K valley, where they interfere as if coming from two identical paths. Typical results are shown in Fig. 5, where (a)–(d) and (e)–(h) depict the numerical and experimental results, respectively, and both the spectra and interferograms before and after the lattice deformation are presented for direct comparison. Although the geometrical paths for light coming from the equivalent valleys [two bright spots in the spectrum, as shown in Fig. 5(e)] are the same, the interference pattern clearly displays an offset due to the action of the deforming beam, which gives rise to an artificial gauge field that brings about an appreciable phase shift. We point out that the Gaussian index profile superimposed to the HCL potential in the induced photonic graphene represents an optical analogy of the out-of-plane deformation of the graphene sheet from a "Gaussian bump" described in [11,34,35]. Experimentally, it is difficult to measure the phase shift as a function of the deformation strength. Although the underlying theory for our optically induced deformation in HCLs is yet to be developed, these results indicate the existence of AB-like interference analogous to those predicted in [11].

It should be pointed out that, in the case of single-beam excitation, no vortex generation is observed in uniform HCLs since both sublattices are equally excited, leading to the degeneracy of

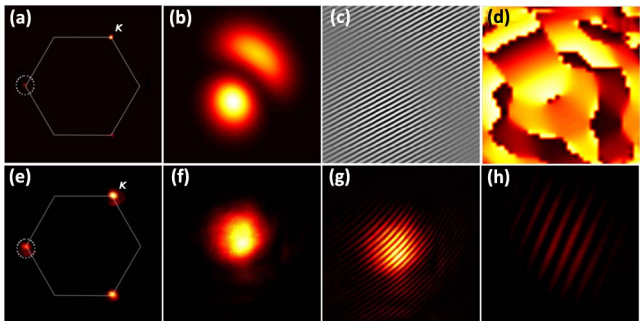

Fig. 3. Probing the HCLs with single-valley excitation before introducing deformation. (a)–(d) and (e)–(h) are the numerical simulations and experimental results, respectively. (a) and (e) depict the Fourier spectrum of the probe beam after propagating through the lattice, while its input spectrum is momentum matched to a K valley. (b) and (f) are the beam patterns of one of the Bragg-reflected spectral components [marked by dashed circles in (a) and (e)]. (c) and (g) are the interferograms between a tilted broad beam (quasi-plane wave) and the beam shown in (b) and (f), showing no topological charge. (d) is the phase diagram of the beam shown in (b), and (h) is the interferogram of the two Bragg-reflected components by filtering out the input components in k-space, showing again no vorticity.

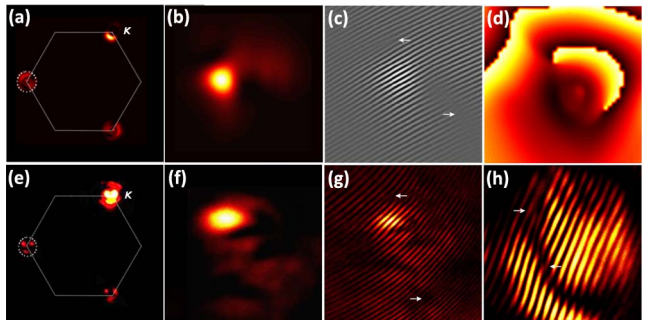

Fig. 4. Probing the HCLs with single-valley excitation with local deformation. All experimental conditions (and, thus, the figure captions) remain the same as in Fig. 3, except for introducing a deforming beam described in Fig. 1. The generation of a vortex pair is evident due to deformation which lifts the degeneracy. The white arrows in Figs. (c), (g), and (h) serve as an eye-guide for the location of generated vortices.

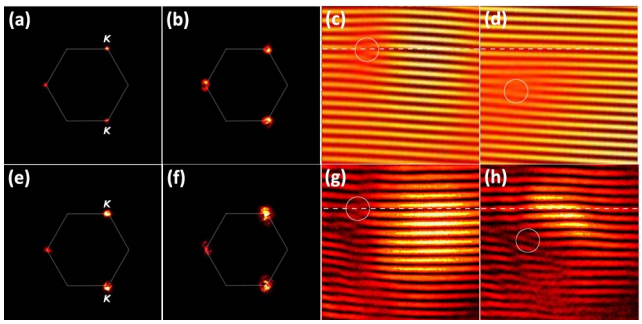

Fig. 5. Probing the HCLs with two-valley excitation before and after introducing deformation. (a)–(d) and (e)–(h) are numerical and experimental results, respectively. (a) and (e) depict the Fourier spectrum of the probe beam after propagating through the undeformed lattice, while at input only the two marked K valleys are initially excited. (b) and (f) are the corresponding results with lattice deformation. (c), (g) and (d), (h) are the interferograms obtained by interfering a plane wave with the Bragg-reflected component at the third K valley before and after introducing the deformation, respectively, where there is a clear shift of vortex position (fringe bifurcation).

the pseudospin states. In this case, the deformation leads to the lifting of topological vortex degeneracy, shifting the vortices to opposite directions. On the other hand, in the case of two-beam excitation, a vortex is observed even in the uniform lattice [Figs. 5(c) and 5(g)], corresponding to the selective excitation of one of the pseudospin states (sublattice degree of freedom) [27]. In the latter case, the deformation leads to the shifting of the vortex location, which may result from the phase shift introduced by the deformation-induced gauge field.

We have demonstrated, both experimentally and numerically, using a simple yet effective platform of optically induced HCLs and lattice deformation, topological vortex degeneracy lifting and Aharonov–Bohm-like interference from local deformation in photonic graphene. The introduction of synthetic magnetic effects in optical systems opens the door to a wide range of new physical effects and applications. Our approach may be adopted to tackle many interesting fundamental questions. For example, can a pseudomagnetic field be observed using strain in a photonic crystal slab geometry (that is, a two-dimensional geometry with a finite height in the third direction) or in a fully three-dimensional photonic crystal for control of the high density of states? Can terahertz generation be enhanced in photonic crystals via strain? Can lasing thresholds in photonic crystals be reduced via engineering pseudomagnetic fields? What is the nonlinear enhancement associated with the Landau levels? The strained photonic lattice provides an excellent experimental setting for probing both linear and nonlinear effects of magnetism in optics. Furthermore, the recent observation of parity-time (PT) symmetry breaking in optics [36,37] has very intriguing implications in honeycomb PT-symmetric lattices, which suggests that the strained honeycomb lattice may provide a context for understanding the effect of magnetism on the PT transition, and on non-Hermitian optics in general.

Funding. National Science Foundation (NSF) (PHY-1404510, EFMA-1542741); Army Research Office (ARO) (W911NF-16-1-0503, W911NF-15-1-0413); National Natural Science Foundation of China (NSFC) (61675168).

REFERENCES

1. K. Novoselov, A. K. Geim, S. Morozov, D. Jiang, M. Katsnelson, I. Grigorieva, S. Dubonos, and A. Firsov, Nature **438**, 197 (2005).
2. Y. Zhang, Y. W. Tan, H. L. Stormer, and P. Kim, Nature **438**, 201 (2005).
3. A. H. Castro Neto, F. Guinea, N. M. R. Peres, K. S. Novoselov, and A. K. Geim, Rev. Mod. Phys. **81**, 109 (2009).
4. M. Polini, F. Guinea, M. Lewenstein, H. C. Manoharan, and V. Pellegrini, Nat. Nanotechnol. **8**, 625 (2003).
5. O. Peleg, G. Bartal, B. Freedman, O. Manela, M. Segev, and D. N. Christodoulides, Phys. Rev. Lett. **98**, 103901 (2007).
6. R. A. Sepkhanov, Y. B. Bazaliy, and C. W. J. Beenakker, Phys. Rev. A **75**, 063813 (2007).
7. L. Duca, T. Li, M. Reitter, I. Bloch, M. Schleier-Smith, and U. Schneider, Science **347**, 288 (2015).
8. N. Fläschner, B. Rem, M. Tarnowski, D. Vogel, D.-S. Lühmann, K. Sengstock, and C. Weitenberg, Science **352**, 1091 (2016).
9. F. Guinea, M. I. Katsnelson, and A. K. Geim, Nat. Phys. **6**, 30 (2010).
10. N. Levy, S. A. Burke, K. L. Meaker, M. Panlasigui, A. Zettl, F. Guinea, A. H. Castro Neto, and M. F. Crommie, Science **329**, 544 (2010).
11. F. de Juan, A. Cortijo, M. A. H. Vozmediano, and A. Cano, Nat. Phys. **7**, 810 (2011).
12. J. Dalibard, F. Gerbier, G. Juzeliūnas, and P. Öhberg, Rev. Mod. Phys. **83**, 1523 (2011).
13. I. Bloch, J. Dalibard, and S. Nascimbene, Nat. Phys. **8**, 267 (2012).
14. N. Goldman, G. Juzeliūnas, P. Öhberg, and I. B. Spielman, Rep. Prog. Phys. **77**, 126401 (2014).
15. R. O. Umucalilar and I. Carusotto, Phys. Rev. A **84**, 043804 (2011).
16. K. Fang, Z. Yu, and S. Fan, Nat. Photonics **6**, 782 (2012).
17. E. Li, B. J. Eggleton, K. Fang, and S. Fan, Nat. Commun. **5**, 3225 (2014).
18. L. D. Tzuang, K. Fang, P. Nussenzveig, S. Fan, and M. D. Lipson, Nat. Photonics **8**, 701 (2014).
19. T. Ochiai and M. Onoda, Phys. Rev. B **80**, 155103 (2009).
20. M. J. Ablowitz, S. Nixon, and Y. Zhu, Phys. Rev. A **79**, 053830 (2009).
21. O. Bahat-Treidel, O. Peleg, M. Grobman, N. Shapira, M. Segev, and T. Pereg-Barnea, Phys. Rev. Lett. **104**, 063901 (2010).
22. C. Fefferman and M. Weinstein, J. Am. Math. Soc. **25**, 1169 (2012).
23. Y. Plotnik, M. C. Rechtsman, D. Song, M. Heinrich, J. M. Zeuner, S. Nolte, N. Malkova, J. Xu, A. Szameit, Z. Chen, and M. Segev, Nat. Mater. **13**, 57 (2014).
24. M. C. Rechtsman, Y. Plotnik, J. M. Zeuner, D. Song, Z. Chen, A. Szameit, and M. Segev, Phys. Rev. Lett. **111**, 103901 (2013).
25. M. C. Rechtsman, J. M. Zeune, A. Tünnermann, S. Nolte, M. Segev, and A. Szameit, Nat. Photonics **7**, 153 (2013).
26. M. C. Rechtsman, J. M. Zeuner, Y. Plotnik, Y. Lumer, D. Podolsky, F. Dreisow, S. Nolte, M. Segev, and A. Szameit, Nature **496**, 196 (2013).
27. D. Song, V. Paltoglou, S. Liu, Y. Zhu, D. Gallardo, J. Xu, M. Ablowitz, N. K. Efremidis, and Z. Chen, Nat. Commun. **6**, 6272 (2015).
28. Y. Aharonov and D. Bohm, Phys. Rev. **115**, 485 (1959).
29. Y. Gao, D. Song, S. Chu, and Z. Chen, IEEE Photonics J. **6**, 2201806 (2014).
30. G. Bartal, O. Cohen, H. Buljan, J. W. Fleischer, and M. Segev, Phys. Rev. Lett. **94**, 163902 (2005).
31. M. Mecklenburg and B. C. Regan, Phys. Rev. Lett. **106**, 116803 (2011).
32. M. Trushin and J. Schliemann, Phys. Rev. Lett. **107**, 156801 (2011).
33. K. Sasaki and R. Saito, Prog. Theor. Phys. Suppl. **176**, 253 (2008).
34. U. Leonhardt, Science **312**, 1777 (2006).
35. J. B. Pendry, D. Shurig, and D. R. Smith, Science **312**, 1780 (2006).
36. A. Szameit, M. C. Rechtsman, O. Bahat-Treidel, and M. Segev, Phys. Rev. A **84**, 021806(R) (2011).
37. K. G. Makris, R. El-Ganainy, D. N. Christodoulides, and Z. H. Musslimani, Phys. Rev. Lett. **100**, 103904 (2008).

130.36.64.29 {ts '2018-08-02 15:06:33'}